

Article

Microstructure and Nanoindentation Evolution of (Ni,Pt)Al Coating on IC21 Substrate at 1100 °C

Yingkun Liu ^{1,2,3}, Yun Ye ^{2,*}, Bin Yin ², Chunming Deng ^{2,*} , Min Liu ^{1,2,*} and Chaoqun Wu ³

¹ College of Materials and Energy, Guangdong University of Technology, Guangzhou 510006, China; liuyingkun@gzfenxi.com

² National Engineering Laboratory for Modern Materials Surface Engineering Technology, The Key Laboratory of Guangdong for Modern Surface Engineering Technology, Institute of New Materials, Guangdong Academy of Sciences, Guangzhou 510651, China; yinbin@gdinm.com

³ Center of Industrial Analysis and Testing, Guangdong Academy of Sciences, Guangzhou 510651, China; qun95@126.com

* Correspondence: hwoods81@126.com (Y.Y.); dengchunming@gdinm.com (C.D.); liumin_gz@163.net (M.L.)

Abstract: In this study, a ~20 μm (Ni,Pt)Al coating was applied to an IC21 substrate via electroplating followed by aluminizing. A thermal exposure test at 1100 °C in air was used to investigate the microstructure evolution and nanoindentation behavior of samples with and without coating. The experimental results show that the (Ni,Pt)Al coating caused a phase change from β-(Ni,Pt)Al to Ni₃Al, and the Topologically Close-Packed (TCP) phase at the interdiffusion zone grew larger after thermal exposure for 200 h at 1100 °C, while a layer of γ' phase was formed on the surface of the IC21 substrate. The nanoindentation test indicated that the elastic modulus was reduced in both annealed samples (with and without coating), and after annealing the sample with coating had higher elastic modulus than the sample without coating. This result reveals that the coating effectively prevented the precipitation of refractory metal elements and the coarsening of the microstructure in the substrate, and thus shows that the coating had advantages not only in terms of improving the high-temperature oxidation properties of the substrate, but also played a significant role in improving the mechanical properties of the substrate.

Keywords: (Ni,Pt)Al coating; IC21 superalloy; nanoindentation; microstructure



Citation: Liu, Y.; Ye, Y.; Yin, B.; Deng, C.; Liu, M.; Wu, C. Microstructure and Nanoindentation Evolution of (Ni,Pt)Al Coating on IC21 Substrate at 1100 °C. *Coatings* **2022**, *12*, 796. <https://doi.org/10.3390/coatings12060796>

Academic Editors: Alessio Lamperti and Sakari Rupp

Received: 8 April 2022

Accepted: 31 May 2022

Published: 8 June 2022

Publisher's Note: MDPI stays neutral with regard to jurisdictional claims in published maps and institutional affiliations.



Copyright: © 2022 by the authors. Licensee MDPI, Basel, Switzerland. This article is an open access article distributed under the terms and conditions of the Creative Commons Attribution (CC BY) license (<https://creativecommons.org/licenses/by/4.0/>).

1. Introduction

With the continuous increase in turbine inlet temperature, turbine blade material requirements are becoming more and more stringent. Ni-based single-crystal superalloy has excellent comprehensive properties at high temperature and is preferred for turbine blades. IC21 is an intermetallic compound superalloy (Ni₃Al based), which is widely used as a structural material in advanced gas turbine engines. The superalloy is usually complex and often contains different alloying elements [1–3]. The refractory metal additions have not only improved the high-temperature mechanical properties, but also enhanced their oxidation/hot corrosion resistance performance.

The (Ni,Pt)Al coatings are widely applied to protect the superalloys from oxidation and hot corrosion due to their excellent properties, such as high melting point, low density, and favorable mechanical properties at high temperature [4,5]. Compared with normal NiAl coating, the presence of Pt can promote the formation of Al₂O₃, enhancing the adhesion of oxide, relieve the detrimental effect of S, reserve greater amounts of Al by its affinity to Al, and restrain the diffusion of refractory alloying elements [6].

The (Ni,Pt)Al coating is prepared via three steps, the electroplating of 3~10 μm Pt, an inert-atmosphere interdiffusion heat treatment, and an aluminizing diffusion treatment [7,8]. Many studies have confirmed that the (Ni,Pt)Al coating can improve the oxidation resistance of the superalloy [9–11].

The coating has a very protective effect on the high-temperature oxidation resistance of the substrate, as widely reported in the literature [10,11]. However, due to the composition differences between the coating and substrate, the diffusion of elements occurs during process at high temperature, which causes TCP phase formation at the interface between the coating and the substrate. The TCP phase dramatically reduces the mechanical properties of the substrate [12,13]. In the previous works related to (Ni,Pt)Al coating, significant effort has been focused on the high-temperature oxidation behavior [14,15], including the microstructure evolution and the effect of different elements (such as Pt, Re, Zr, etc.) on the thermal oxidation resistance of the coating, but studies on the change in the mechanical properties in the (Ni,Pt)Al coating caused by diffusion at high temperature are few [16,17]. The coated superalloy system has been widely used in surface protection and life extension [18,19]. However, in a high-temperature environment, reduced mechanical properties and oxidation are two important factors leading to failure [20,21]. Therefore, the study of the interdiffusion between coating and substrate and its effect on the mechanical properties of the coating system is of great significance for guiding the design of coatings and predicting the high-temperature life of coated parts in the aerospace field.

Zimin Zhou et al. [22] investigated the microstructures and cyclic oxidation behavior of the β -NiAlCrSi coatings at 1200 °C with 0.1 Dy single-doping, low-Pt single-doping and low-Pt/0.1 Dy co-doping, and the results show that the addition of low-Pt effectively suppressed the precipitation of TCP phases in the coatings during heat treatment. H. Liu et al. [23] reported that better oxidation performance was observed in the NiRePtAl coating, which showed lower rates of oxide growth and phase degradation. Y.F. Yang et al. [6] investigated the cyclic oxidation behavior of (Ni,Pt)Al coating and confirmed that the addition of Pt in B2-structured NiAl can significantly slow down the oxidation rate at high temperature, while the decreased oxide growth rate was attributed to the formation of dual-layered α -Al₂O₃ containing Pt-rich precipitates at grain boundaries.

In this paper, Scanning Electron Microscope (SEM), Energy Disperse Spectroscopy (EDS), Electron Probe Microanalysis (EPMA) and X-Ray Diffraction (XRD) were used for characterizing the microstructure evolution and the nanoindentation was used to investigate the mechanical properties of the samples with and without (Ni,Pt)Al coating before and after 200 h of thermal exposure. By comparing the results, the paper aims to connect and review the relationship between the microstructure evolution and mechanical properties.

2. Materials and Methods

2.1. Preparation of (Ni,Pt)Al Coating

A Ni₃Al-based single-crystal superalloy IC21 was utilized as the substrate material, and its chemical composition was measured by inductively coupled plasma optical emission spectrometry (ICP-OES) analysis. The results are shown in [24].

The IC21 substrate was cut into 40 mm × 12 mm × 1 mm using a spark discharging machine and was ground down with 800# SiC paper and then sandblasted. The samples were cleaned using ultrasonic acetone solution and blow-dried.

The acidic electroplating of Pt was conducted in a commonly used solution of K₂ [Pt(NO₂)₂SO₄] at 65 °C with a pH value in the range of 1–2 (adjusted using diluted H₂SO₄). The effective Pt concentration of the solution was approximately 10 g L⁻¹. The composition and deposition conditions of alkaline Pt electroplating are listed in [20]. A Pt layer of 5 μm thickness was deposited onto the specimens. Next, homogenization of the Pt-coated samples was conducted at 1040 °C for 1 h in vacuum (<6 × 10⁻³ Pa) to remove H₂ and dilute the surface concentration of Pt. Finally, the samples underwent low-activity vapor phase aluminizing (VPA) at 1070 °C for 5 h in a vertical above-pack aluminization furnace filled with Ar to yield a single-phase β -(Ni,Pt)Al coating. The aluminizing pack in the current study was composed of 96 wt. % commercially available Fe-49Al (wt. %) powder and 4 wt. % NH₄Cl activators (analytically pure) [8].

2.2. Thermal Exposure Test at 1100 °C

The thermal exposure test was carried out in a furnace in air at 1100 °C. When the temperature of the furnace reached 1100 °C, the samples were placed in the ceramic crucible and then into the furnace for different times. For comparison, samples of the same size from pristine substrate were also placed into the furnace.

2.3. Characterizations

The morphology and chemical compositions of the samples were characterized using an Electron Probe Microanalysis (EPMA, JXA-8100, JEOL, Tokyo, Japan) equipped with an Energy Dispersive Spectrometer (EDS, X-Max20, Oxford, UK). X-ray diffraction (Smart Lab, Rigaku, Tokyo, Japan) was used to study the phase changes in the coatings under different oxidation times, using Cu K α -ray as the diffraction source with a scanning step of 0.02°/s and a scanning range of 2 θ from 10° to 90°.

The nanoindentation test was conducted by Anton Paar NHT3 using a Berkovich diamond indenter. All the samples were analyzed in cross-section. The measurements were performed in a line of 45° from the substrate toward the coating and with a distance of 15 μ m between the two measured points. The measurements were performed at a constant load of 10 mN. In addition to conventional hardness data, the stiffness, elastic modulus and other mechanical properties of the material can be obtained through the continuous change in load controlled by a computer and the on-line monitoring of the depth of indentation.

3. Results and Discussion

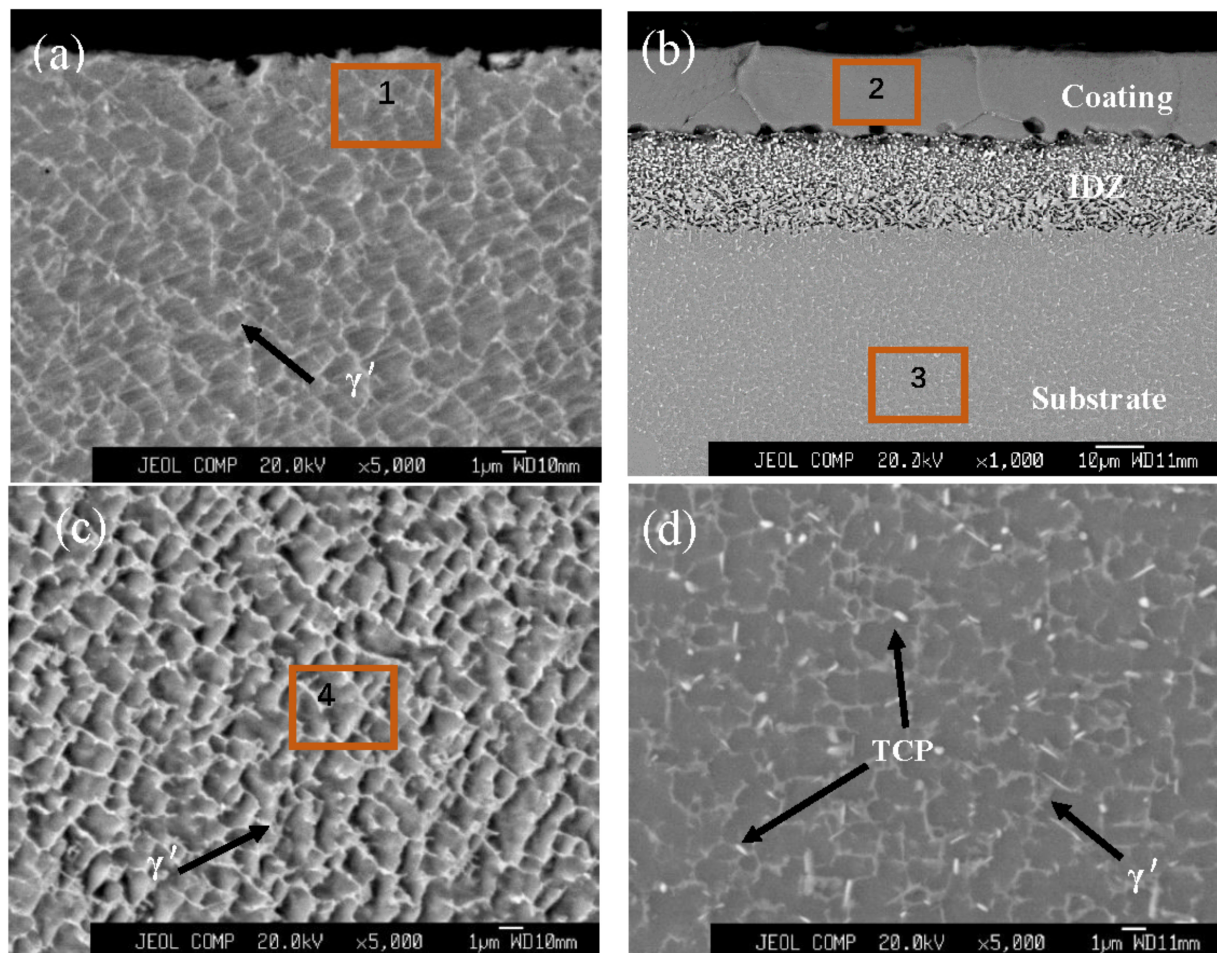
3.1. Cross-Section Morphology with and without Coating before Thermal Exposure

The cross-sectional microstructure of the samples before thermal exposure is shown in Figure 1. The microstructure of the substrate showed homogeneous ($\gamma + \gamma'$) phase, and few TCP phases (Figure 1a,c). After coating preparation, there was an obvious interdiffusion zone (IDZ, about 20 μ m) between the coating and substrate, shown in Figure 1b. In this area, many granular and needle-like TCP phases can be seen. Some granular TCP phases can also be seen in the substrate close to the coating, as shown in Figure 1d. The EDS analysis results in the red box in Figures 1–3 reveal that the TCP phases were rich in Mo, Re and Cr, as shown in Table 1. As reported in the literature [25], the TCP phase is a topological close-packed phase with a complex structure. Compared with Figure 1c, the γ' phase in Figure 1d is larger, and there is more TCP phase in the substrate. This indicates that in the process of coating preparation, especially in the aluminizing stage, high temperature and mutual diffusion lead to the growth of γ' and the precipitation of TCP phase [11]. For the superalloy, the fine and staggered distribution ($\gamma + \gamma'$) phase is very important, which is helpful for the creep resistance and lifetime of the material [26]. Because of the high-temperature treatment during coating preparation, the γ' phase grew larger and some TCP phases separated out from the substrate, which consumed the refractory metallic elements. The refractory metallic element is the solid-solution-strengthening element in the substrate, the gathering of which is disadvantageous to the mechanical properties of the substrate.

The EDS results in Table 1 show that the IC21 substrate had a uniform distribution of composition and although the IDZ zone was introduced in the coating preparation process, the substrate composition of the sample with (Ni,Pt)Al coating is consistent with that of the sample without coating.

Table 1. Chemical compositions of the marked areas in Figures 2 and 3 (wt. %) by EDS.

	Al	Cr	Ni	Mo	Ta	Re	Pt
1	6.99	1.66	77.40	10.28	2.74	0.93	/
2	21.61	1.77	70.76	0.31	0.30	/	4.94
3	7.45	1.75	76.54	10.39	3.12	0.75	/
4	7.30	1.76	77.28	10.32	2.69	0.65	/
5	17.77	1.91	77.08	1.25	0.34	0.41	1.24
6	17.83	1.81	76.86	1.75	/	/	1.74
7	11.02	1.24	79.88	3.27	3.39	/	1.21
8	8.97	1.75	73.19	10.83	3.15	0.41	1.69
9	11.44	1.40	79.93	3.03	/	0.38	3.82
10	4.59	2.25	75.71	13.28	2.07	2.10	/
11	4.64	2.39	75.50	13.58	1.90	2.00	/
12	4.56	2.24	74.76	13.72	1.63	2.86	/
13	8.13	0.69	79.31	6.05	4.66	1.25	/
14	7.29	1.52	76.76	10.22	2.85	1.37	/
TCP	1.46	2.66	30.07	39.92	/	25.85	/

**Figure 1.** The backscattered electron image of the cross-section of (a,c) IC21 substrate, and (b,d) with coating before thermal exposure.

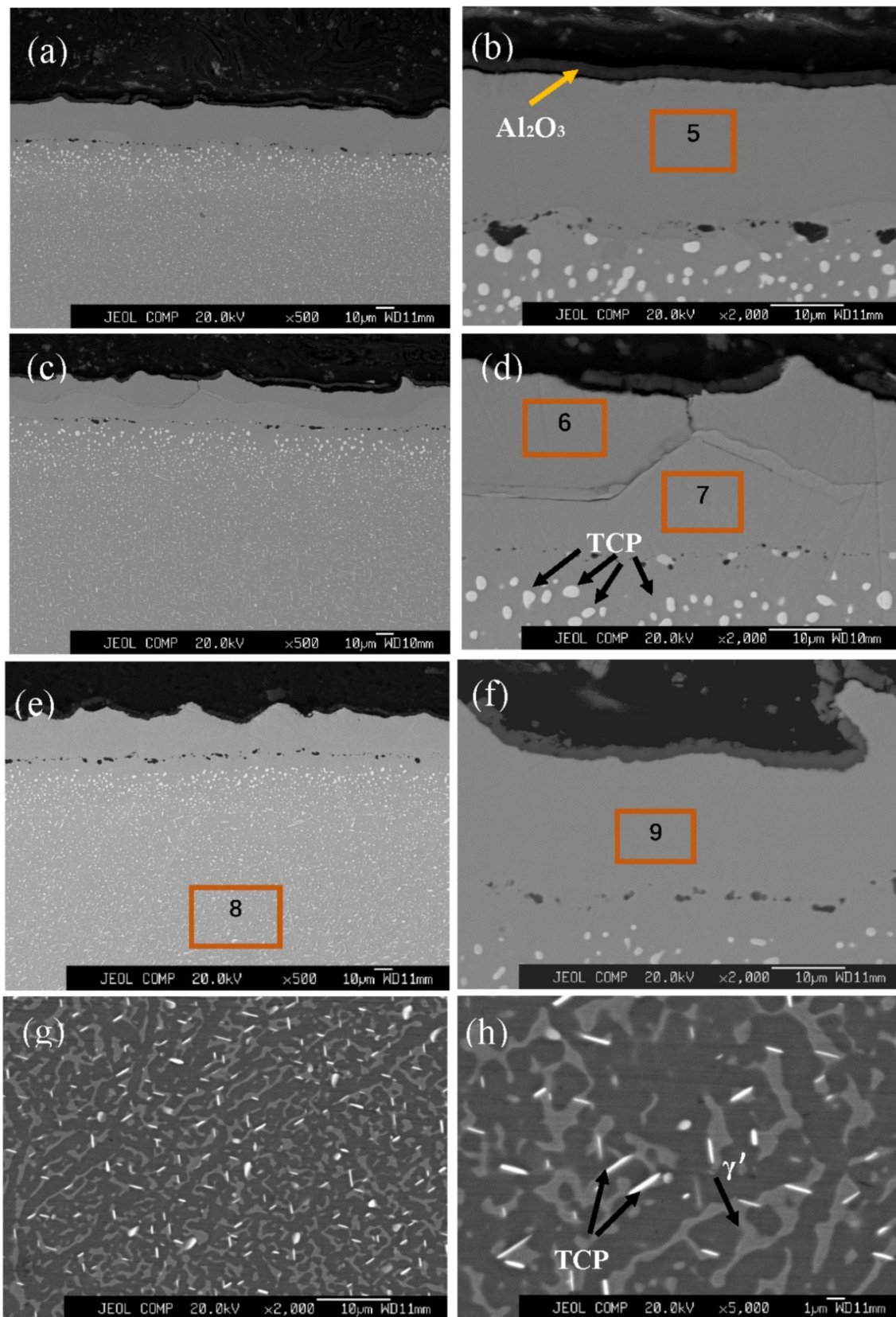


Figure 2. The cross-section morphology of IC21 substrate with coating after 50 h (a,b), 150 h (c,d), 200 h (e–h) after thermal exposure.

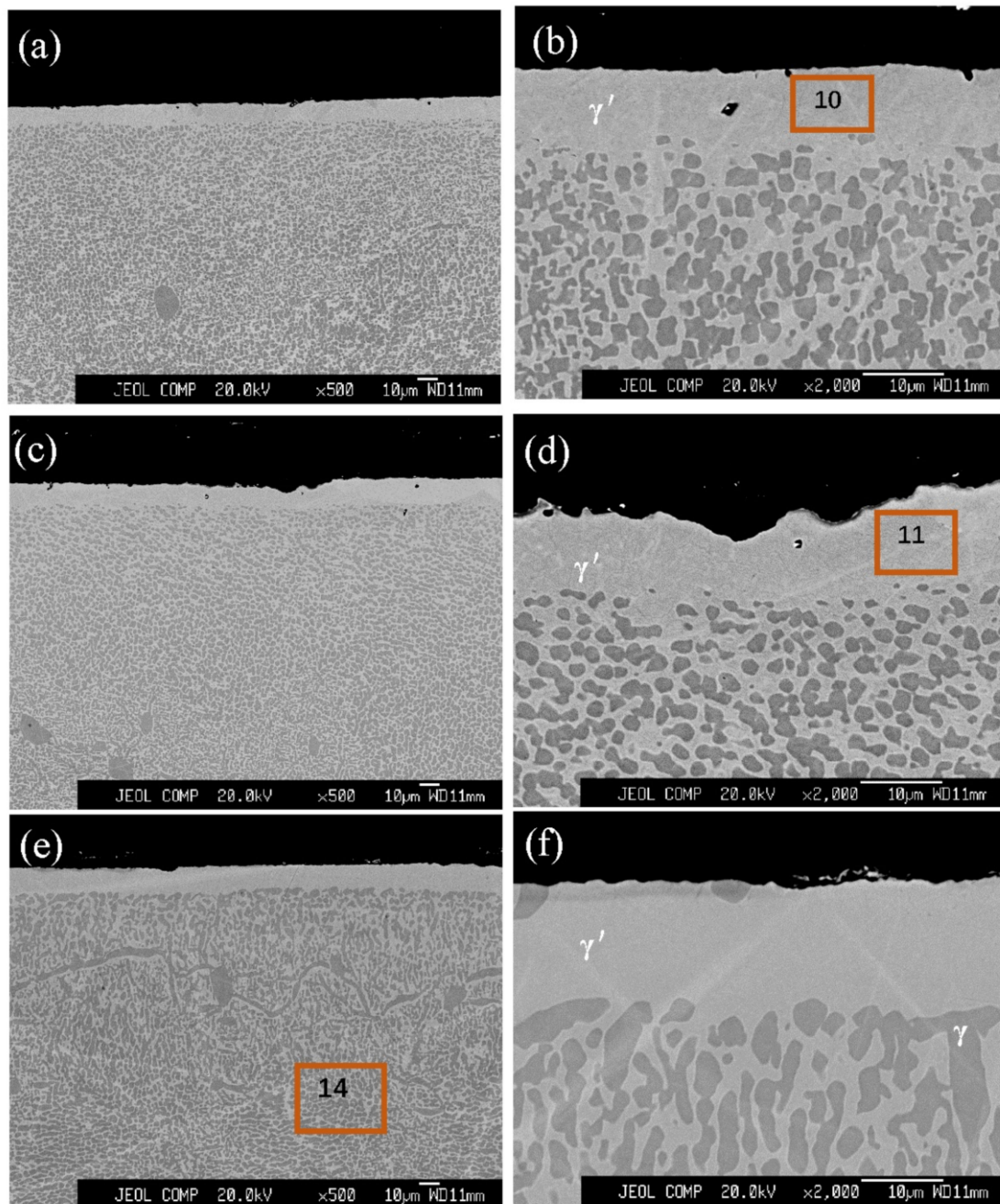


Figure 3. The cross-section morphology of IC21 substrate without coating after 50 h (a,b), 150 h (c,d) and 200 h (e,f) thermal exposure.

3.2. Cross-Section Morphology with and without Coating after Thermal Exposure

The cross-sectional microstructure of the IC21 substrate with (Ni,Pt)Al coating thermally exposed for different length of time is shown in Figure 2. Compared with Figure 1c, the size of TCP phase grew bigger during thermal exposure. The volume content of TCP in the substrate area (calculated using Image Pro) was about 20.8%, 20 times that of the sample without annealing.

As shown in Figure 2b,d,f, visible spallation of the alumina scale occurred on the coating surface and a thin and continuous α -Al₂O₃ scale was formed on the coating as well. The TCP phases were distributed throughout the whole sample, shown as white particles in the IDZ zone and appearing needle-like in the substrate. The TCP phases grew in size and number [27]. It can be seen clearly in Figure 2d that the coating was divided into two layers.

According to the results of EDS analysis (Table 1) and XRD (Figure 4), the upper layer containing more aluminum should be β -(Ni,Pt)Al and the lower layer should be the Ni₃Al. NiAl and Ni₃Al are both high temperature structural materials with a high melting point. Ni₃Al is a face-centered cubic structure with a melting point of about 1400 °C, while NiAl is a body-centered cubic structure with a melting point of about 1640 °C. NiAl has a higher melting point and more advantages in terms of high-temperature oxidation resistance [28].

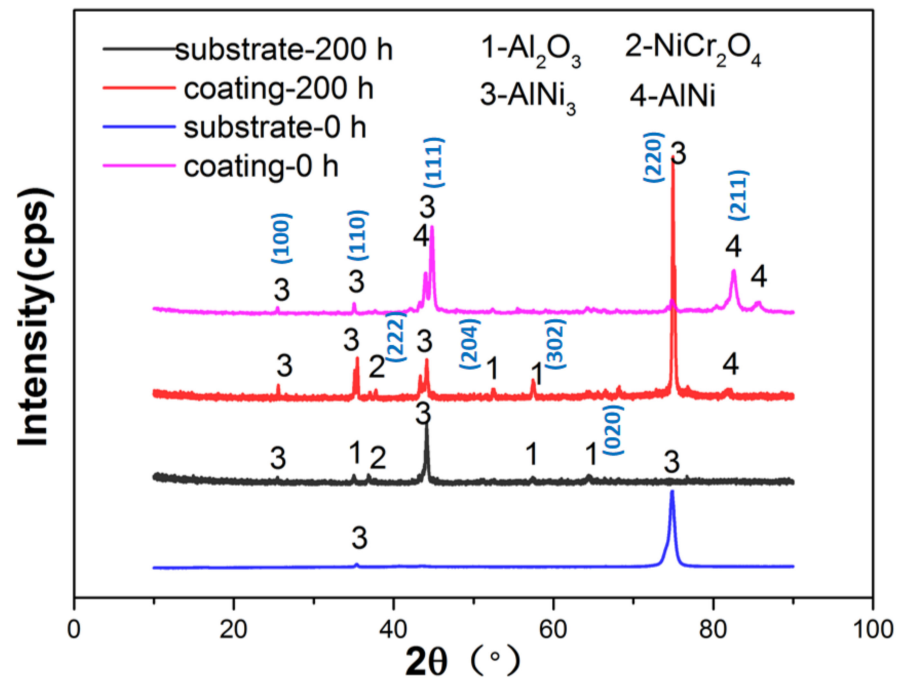


Figure 4. X-ray diffraction patterns of the samples before and after thermal exposure test.

The EDS results suggest that the (Ni,Pt)Al coating underwent a phase change from β to γ' . Al content decreased from 21% to 11% and the Mo content increased from 0.31% to 3.27% (in wt. %). It can be clearly seen that the microstructure (Figure 2g,h) maintained a meticulous organization after 200 h of thermal exposure, exhibiting good microstructural stability at high temperature.

As shown in Figure 3a,b, after 50 h of thermal exposure, the tiny, regular $\gamma + \gamma'$ phase was destroyed and became coarser and inhomogeneous. A $\sim 10 \mu\text{m}$ uniform and continuous γ' is observed on the surface, and the thickness had no significant change at different thermal exposure times. The EDS results show that the Al content on the surface was reduced to 4.5~5 (wt. %) after thermal exposure. During the thermal exposure, Al in the coating combined with O in air, forming Al₂O₃ on the surface, resulting in the decrease in Al content on the surface area. The deterioration rate of the β -AlNi phase is dependent on the initial Al content of the coating and the rate of Al consumption. The aluminum oxide formed during the initial stages of oxidation undergoes transformations through a series of transitional metastable alumina polymorphs, such as γ -Al₂O₃ and θ -Al₂O₃, before transforming into the stable α -Al₂O₃ phase [29]. The lower Al content caused the surface to change to a γ' phase, containing less Al.

Compared with the sample with (Ni,Pt)Al coating, the sample of IC21 substrate had a lower Al content on the sample surface. During the thermal exposure test, sufficient Al in the coating provided the formation of a continuous α -Al₂O₃ layer on the surface.

It is well known that superalloys have excellent mechanical properties at high temperatures due to their finely dispersed $\gamma + \gamma'$ phase. For the IC21 substrate, the size of the γ' phase increased after thermal exposure, and the resistance of the grain boundary slip deformation (i.e., dislocation movement) decreased, which had a destructive effect on the mechanical properties of the superalloy. The coarsening of the coated sample after thermal

exposure is not as serious as that of the uncoated sample, which indicates that the coating is able to reduce the rafting of the substrate.

Figure 4 shows the XRD patterns of the two samples with and without coating before and after 200 h thermal exposure at 1100 °C. For the IC21 substrate, the maximum peak occurred only at approximately 75°, which confirmed that the material was a single superalloy. After the thermal exposure test, the oxides on the sample surface were both composed of α -Al₂O₃. The main phases were AlNi₃ in both the substrate and the coating, revealing a phase transformation of the coating during the thermal exposure test.

Figure 5 shows the elemental distributions of the sample with coating before and after 200 h thermal exposure test. The Al content in the coating before the test was ~25 wt. %, and the Al content was reduced to ~12 wt. % after thermal exposure for 200 h. However, the Al content in the substrate was not significantly changed, indicating that the Al in the coating was mainly diffused to the surface for the formation of the Al₂O₃ layer.

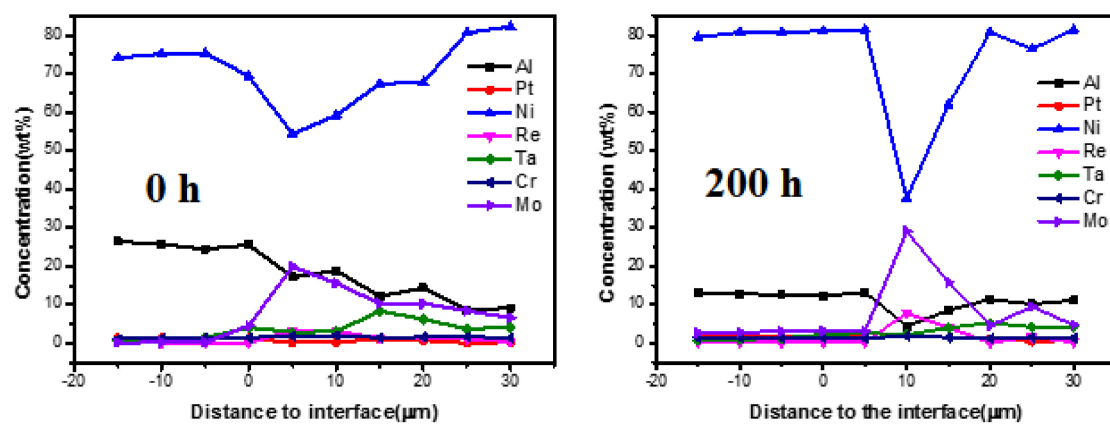


Figure 5. The elemental distributions of the samples before (0 h) and after 200 h thermal exposure by EPMA.

The diffusion of Cr, Mo, and Ta elements from the substrate to the coating can be seen in Figure 5, revealing that after 200 h of thermal exposure, the content of Mo in some areas of the coating reached 2.83%. After 200 h of diffusion, 0.16 wt. % of Re was measured in the coating, indicating the diffusion of Re from the substrate to the coating.

3.3. Micro Hardness and Nanoindentation

The stability of mechanical properties at a high temperature of superalloy has a vital impact on its service life. For macroscopic materials, the overall mechanical parameters of the material can be obtained by high-temperature tensile tests. However, in the case of the mutual diffusion of coating and superalloy, the mechanical performance changes caused by mutual diffusion cannot be achieved in such a macroscopic way, and the nanoscale indentation has an irreplaceable advantage in this regard. With regard to the nanoindentation, it can not only characterize the hardness at the nanoscale, but also characterize the elastic modulus, fracture toughness, strain hardening effect, and viscoelastic or creep behavior of materials, so it has been widely used in the field of materials science [30–33].

Figure 6 shows the typical load–unload curves of the different phases before and after the thermal exposure test. With the same indentation condition, the TCP phase showed the smallest indentation depth. The measured values of the elastic modulus in TCP were more than 300 GPa, which was much larger than the other phase. The TCP phase is a complex crystal structure consisting of a high stacking density of refractory metal elements and a variety of coordination polyhedrals, so it has a high elastic modulus. Due to the interdiffusion, the coating obtained more refractory elements after the test, resulting in an increase in elastic modulus, showing a shallower indentation depth (green curve in Figure 6).

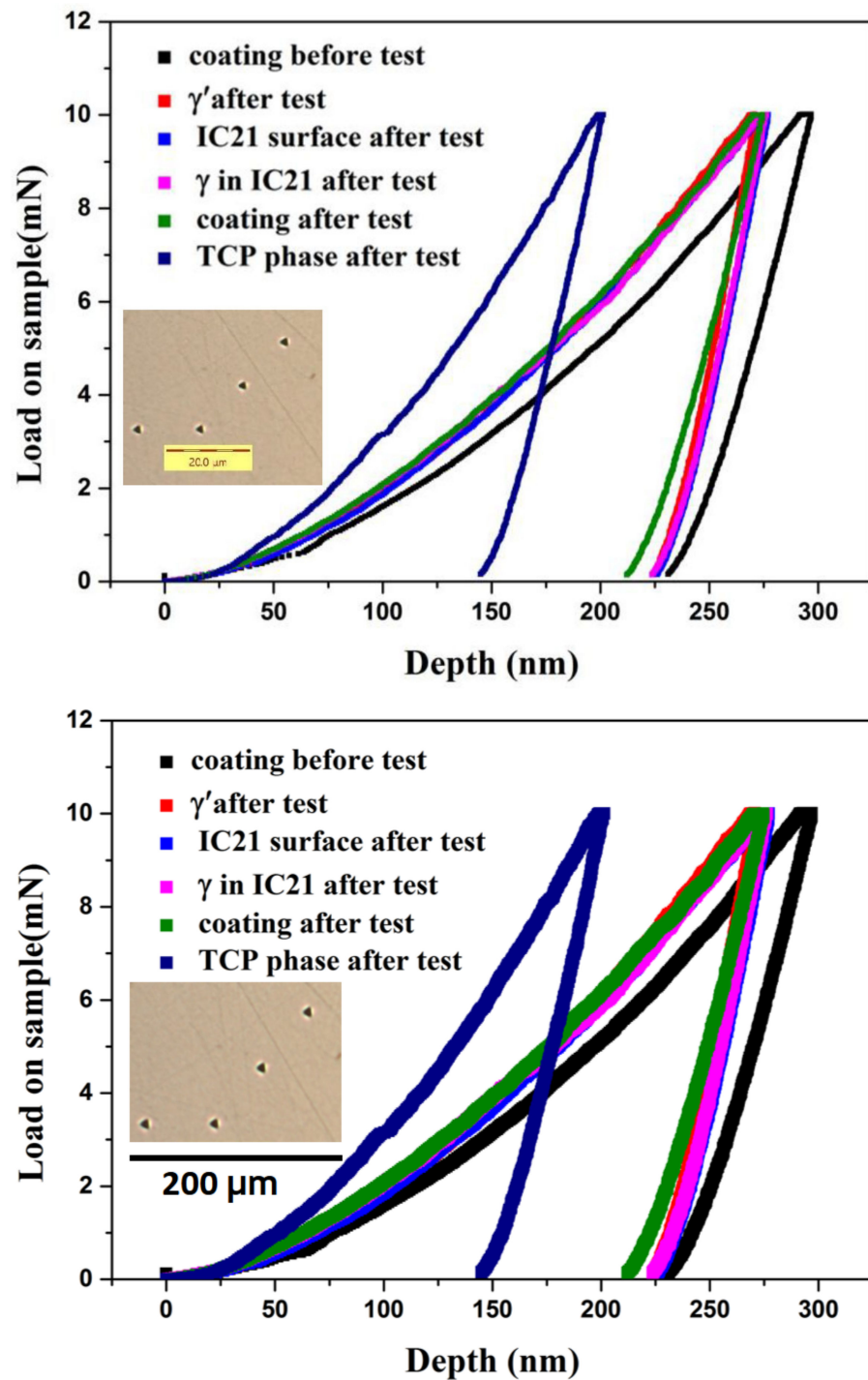


Figure 6. The load–displacement curves of different phases.

Figure 7a shows the microhardness of the samples in the substrate area. After coating preparation, the microhardness was reduced from 388 to 373. This can be explained by the fact that the precipitation of the TCP phase results in the decrease in refractory metal elements in the substrate, leading to a decrease in hardness. The microstructure refinement and solid-solution strengthening of refractory elements are the main reasons for the high hardness of the materials [34]. After thermal exposure, the microstructure became progressively coarser, resulting in a decrease in hardness. After coating preparation, the TCP phase also precipitated out, which weakened the strengthening effect of the refractory elements and led to a decrease in hardness (Figure 7 3#). Compared with the microhardness

of 2# and 4# in Figure 7, the sample with coating did not show a sharp reduction, revealing a hardness stability.

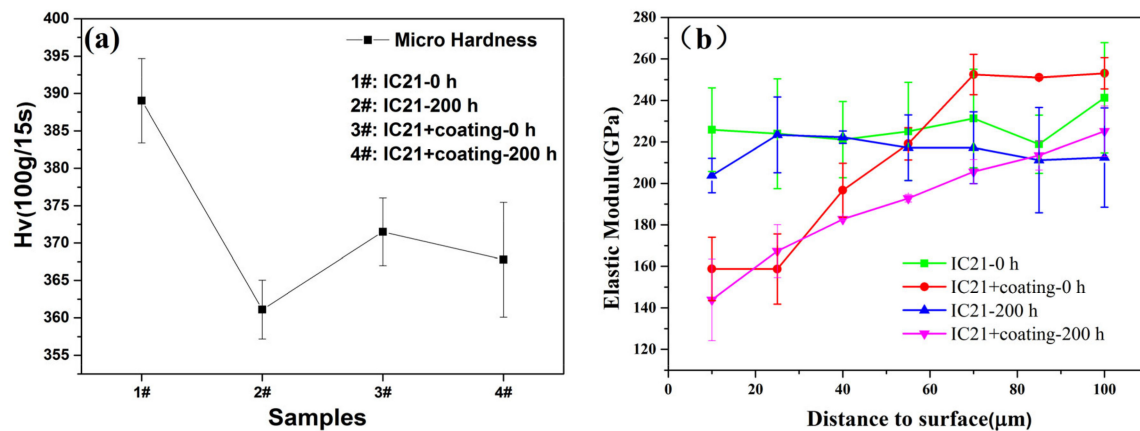


Figure 7. The results of the microhardness of the substrate area (a) and the elastic modulus of the samples (b).

The elastic modulus can be regarded as an indicator to measure the degree of difficulty in producing elastic deformation of materials. The larger the value is, the greater the stress that causes certain elastic deformation of materials will be. The change in the elastic modulus of a sample at high temperature has an important effect on the service life of the sample. Three nanoindentation tests were performed for each sample. The mean value and variance of the elastic modulus for each sample is shown in Figure 7b.

The IC21 substrate had a uniform elastic modulus [35,36]. After the 200 h test, in addition to the point near the surface, which belonged to the γ phase, the elastic modulus was uniform but exhibited an overall decrease. It has been reported that the fine second phase can enhance the elastic modulus of the material [37,38]. However, after thermal exposure, the residual stress concentration is caused by the uneven distribution of elements due to the coarse structure, which leads to a decrease in the elastic modulus of the sample. After thermal exposure at 1100 °C for 200 h, the elastic modulus of IC21 substrate both with and without coating decreased, indicating the influence of thermal exposures on the superalloy's mechanical properties.

The precipitation and growth of the TCP phase absorbed solid solution strengthening elements (such as Mo, Ta, Re, etc.) in the substrate, which resulted in the decrease in elastic modulus in the substrate. When the substrate deforms at high temperature, the TCP area blocks the deformation, and causes the formation of cracks in the substrate, which greatly reduces its mechanical properties. In the β -NiAl phase, the concentration of Al is the main reason for the decrease in elastic modulus. This behavior was confirmed by nano-indentation measurements on Ni-NiAl diffusion pairs [39]. The composition of the micro-zone had an impact on the elastic modulus of the sample.

The large difference in elastic modulus between the coating and the substrate increases the tendency of stress to concentrate at the interface between the coating and the substrate, which makes it prone to crack during service at high temperature, leading to the decrease in the mechanical properties of the sample. Especially after the thermal exposure test, more needle-like TCP phases formed in the SRZ region, which was the main source of cracks [40,41].

4. Conclusions

A $\sim 20 \mu\text{m}$ (Ni,Pt)Al coating was coated on an IC21 substrate, and the thermal exposure test at 1100 °C was carried out in a furnace exposed to air. Comparing the test results of the substrate with and without coating, the following conclusions can be drawn:

1. Compared with the IC21 substrate, the (Ni,Pt)Al coating formed a continuous dense Al₂O₃ layer on the surface after 200 h of thermal exposure, showing a better resistance to high-temperature oxidation.
2. Although there is TCP phase precipitation, the IC21 substrate with coating showed a tinier microstructure than the pure IC21 substrate after 200 h of thermal exposure, indicating the positive role of coating in maintaining the stability of the substrate.
3. The nanoindentation results show that after thermal exposure at 1100 °C for 200 h, the elastic modulus of the IC21 substrate and the coating was reduced, and the TCP phase showed the biggest elastic modulus of 328 GPa.
4. The sample with (Ni,Pt)Al coating had a uneven distribution of the elastic modulus, which is the main reason for the degradation of the mechanical properties.

Author Contributions: Conceptualization, Y.L. and C.D.; methodology, M.L.; formal analysis, B.Y. and C.W.; investigation, Y.Y.; resources, M.L.; data curation, Y.Y.; writing—original draft preparation, Y.L.; writing—review and editing, C.D. All authors have read and agreed to the published version of the manuscript.

Funding: The research was supported by the projects of the Key-Area Research and Development Programs of Guangzhou (No. 202007020008), the Guangdong Provincial Natural Science Foundation Project (No. 2020A1515010948), the Basic and Applied Basic Research Fund of Guangdong Province (No. 2021A1515011693), and the special fund project of Guangdong Academy of Sciences (No. 2020GDASYL-20200104028).

Institutional Review Board Statement: Not applicable.

Informed Consent Statement: Not applicable.

Data Availability Statement: Not applicable.

Conflicts of Interest: The authors declare no conflict of interest.

References

1. Zheng, Y.R.; Wang, X.P.; Dong, J.X.; Han, Y.F. Superalloys 2000. In Proceedings of the Proof 9th International Symposium on Superalloys, Champion, PA, USA, 17–21 September 2000; TMS: Warrendale, PA, USA, 2000; p. 305.
2. Frazier, D.J.; Whetstone, J.R.; Harris, K.; Erickson, G.L. *High Temperature Materials for Power Engineering*; Kluwer Academic Publishers: Boston, UK, 1990; p. 1281.
3. Waudby, P.E.; Benson, J.M.; Stander, C.M. *Advances in Turbine Materials Design and Manufacturing*; Institute of Materials: London, UK, 1997; p. 322.
4. Tolpygo, V.K.; Clarke, D.R. Rumpling of CVD (Ni,Pt)Al diffusion coatings under intermediate temperature cycling. *Surf. Coat. Technol.* **2009**, *203*, 3278–3285. [[CrossRef](#)]
5. Audigié, P.; Put, A.R.-V.; Malié, A.; Thouron, C.; Monceau, D. High-temperature cyclic oxidation of Pt-rich γ - γ' bond-coatings. Part II: Effect of Pt and Al on TBC system lifetime. *Corros. Sci.* **2019**, *150*, 1–8. [[CrossRef](#)]
6. Yang, Y.F.; Jiang, C.Y.; Yao, H.R.; Bao, Z.B.; Zhu, S.L.; Wang, F.H. Cyclic oxidation and rumpling behaviour of single phase β -(Ni,Pt)Al coatings with different thickness of initial Pt plating. *Corros. Sci.* **2016**, *111*, 162–174. [[CrossRef](#)]
7. Benoist, J.; Badawi, K.F.; Malie, A.; Ramade, C. Microstructure of Pt-modified aluminide coatings on Ni-based superalloys. *Surf. Coat. Technol.* **2004**, *182*, 14–23. [[CrossRef](#)]
8. Yang, Y.F.; Jiang, C.Y.; Bao, Z.B.; Zhu, S.L.; Wang, F.H. Effect of aluminisation characteristics on the microstructure of single phase β -(Ni,Pt)Al coating and the isothermal oxidation behavior. *Corros. Sci.* **2016**, *106*, 43–54. [[CrossRef](#)]
9. Oskay, C.; Rudolphi, M. Evolution of microstructure and mechanical properties of NiAl-Diffusion coatings after themocyclic exposure. *Intermetallics* **2017**, *89*, 22–31. [[CrossRef](#)]
10. Zihao, T.; Lin, Y.; Wang, X.; Du, Y.; Ye, L. Evolution of TCP Phase During Long Term Thermal Exposure in Several Re-Containing Single Crystal Superalloys. *Acta Metall. Sin. (Engl. Lett.)* **2020**, *33*, 731–740.
11. Das, D.K. Microstructure and high temperature oxidation behavior of Pt-modified aluminide bond coats on Ni-base superalloys. *Prog. Mater. Sci.* **2013**, *58*, 151–182. [[CrossRef](#)]
12. Audigié, P.; Put, A.R.-V.; Malié, A.; Monceau, D. High-temperature cyclic oxidation behavior of Pt-rich γ - γ' coatings. Part I: Oxidation kinetics of coated AM1 systems after very long-term exposure at 1100 °C. *Corros. Sci.* **2018**, *144*, 127–135.
13. Jiang, C.; Qian, L.; Feng, M.; Liu, H.; Bao, Z.; Chen, M.; Zhu, S.; Wang, F. Benefits of Zr addition to oxidation resistance of a single-phase(Ni,Pt)Al coating at 1373 K. *J. Mater. Sci. Technol.* **2019**, *35*, 1334–1344. [[CrossRef](#)]
14. Pauletti, E.; d'Oliveira, A.S.C.M. Influence of Pt concentration on structure of aluminized coatings on a Ni base superalloy. *Surf. Coat. Technol.* **2017**, *332*, 57–63. [[CrossRef](#)]

15. Xu, Z.; Wang, Z.; Huang, G.; Mu, R.; He, L. Morphology, bond strength and thermal cycling behavior of (Ni, Pt)Al/YSZ EB-PVD thermal barrier coatings. *J. Alloys Compd* **2015**, *651*, 445–453. [[CrossRef](#)]
16. Ebach-Stahl, A.; Fröhlich, M. Oxidation study of Pt–Al based coatings on γ -TiAl at 950 °C. *Surf. Coat. Technol.* **2016**, *287*, 20–24. [[CrossRef](#)]
17. Oskay, C.; Galetz, M.C.; Murakami, H. Oxide scale formation and microstructural degradation of conventional, Pt and Pt/Ir-modified NiAl diffusion coatings during thermocyclic exposure at 1100 °C. *Corros. Sci.* **2018**, *144*, 313–327. [[CrossRef](#)]
18. Jiang, C.; Qian, L.; Feng, M.; Liu, H.; Bao, Z.; Chen, M.; Zhu, S.; Wang, F. Preparation and Enhanced Hot Corrosion Resistance of a Zr-Doped PtAl₂+(Ni,Pt)Al DuM-Phase Coating. *Acta Metall. Sin.* **2018**, *54*, 581–590.
19. Yang, H.-Z.; Zou, J.-P.; Shi, Q.; Dai, M.-J.; Lin, S.-S.; Du, W.; Lv, L. Analysis of the microstructural evolution and interface diffusion behavior of NiCoCrAlYTa coating in high temperature oxidation. *Corros. Sci.* **2019**, *153*, 162–169. [[CrossRef](#)]
20. Yu, C.T.; Liu, H.; Ullah, A.; Bao, Z.B.; Zhu, S.L.; Wang, F.H. High-temperature performance of (Ni,Pt)Al coatings on second-generation Ni-base single-crystal superalloy at 1100 °C: Effect of excess S impurities. *Corros. Sci.* **2019**, *159*, 108–115. [[CrossRef](#)]
21. Ye, L.Y.; Chen, H.F.; Liu, B.; Yang, G.; Luo, H.J.; Gao, Y.F. Effect of Pt content on initial TGO formation and available Al reserve of Pt-Al coatings during thermal cycling. *Surf. Coat. Technol.* **2018**, *337*, 82–89. [[CrossRef](#)]
22. Zhou, Z.; Peng, H.; Zheng, L.; Guo, H.; Gong, S. Improved oxide scale adherence of low-Pt/Hf co-doped-NiAlCrSi coating on superalloy IC21 at 1200 °C. *Corros. Sci.* **2016**, *105*, 78–87. [[CrossRef](#)]
23. Liu, H.; Xu, M.M.; Li, S.; Bao, Z.B. Improving cyclic oxidation resistance of Ni₃Al-based single crystal superalloy with low-diffusion platinum-modified aluminide coating. *J. Mater. Sci. Technol.* **2020**, *54*, 132–143. [[CrossRef](#)]
24. Liu, Y.; Yin, B.; Deng, C. Microstructure evolution and interdiffusion behaviors of (Ni,Pt)Al coating with and without Re-diffusion barrier on IC21 substrate at 1100 °C. *Mater. Charact.* **2021**, *181*, 222450. [[CrossRef](#)]
25. Anijdan, S.M.; Bahrami, A. A new method in prediction of TCP phases formation in superalloys. *Mater. Sci. Eng. A* **2005**, *396*, 138–142. [[CrossRef](#)]
26. Liu, H.; Li, S.; Jiang, C.Y. Preparation and oxidation performance of a low-diffusion Pt-modified aluminide coating with Re-base diffusion barrier. *Corros. Sci.* **2020**, *168*, 105582. [[CrossRef](#)]
27. Taghipour, M.; Eslami, A.; Salehi, M.; Bahrami, A. An investigation on anti-coking behavior of gas phase aluminide coatings applied on a high performance micro alloyed (HP-MA) steel. *Surf. Coat. Technol.* **2020**, *389*, 125607. [[CrossRef](#)]
28. Mardiha, P.; Bahrami, A.; Mohammadnejad, A. Towards a High Strength Ductile Ni/Ni₃Al/Ni Multilayer Composite using Spark Plasma Sintering. *Sci. Sintering* **2019**, *51*, 401–408. [[CrossRef](#)]
29. Taghipour, M.; Eslami, A.; Bahrami, A. High temperature oxidation behavior of aluminide coatings applied on HP-MA heat resistant steel using a gas-phase aluminizing process. *Surf. Coat. Technol.* **2022**, *434*, 128181. [[CrossRef](#)]
30. Xiao, H.; Wang, X.; Long, C. Theoretical model for determining elastic modulus of ceramic materials by nanoindentation. *Materialia* **2021**, *17*, 101121. [[CrossRef](#)]
31. Dada, M.; Popoola, P.; Mathe, N.; Adeosun, S.; Pityana, S. Investigating the elastic modulus and hardness properties of a high entropy alloy coating using nanoindentation. *Int. J. Lightweight Mater.* **2021**, *4*, 339–345. [[CrossRef](#)]
32. Shen, L.; Septiwerdani, P.; Chen, Z. Elastic modulus, hardness and creep performance of SnBi alloys using nanoindentation. *Mater. Sci. Eng. A* **2012**, *558*, 253–258. [[CrossRef](#)]
33. Gadge, M.; Chincharikar, S. Characterization of pre-and/or post-treated PVD-AlTiN coating: Nanohardness, modulus of indentation and percent elastic portion of the nanoindentation. *Mater. Today Proc.* **2021**, *46*, 8386–8392. [[CrossRef](#)]
34. Fei, G.; Han, Z.; Zhen, Z. Characterization of Solid Solution Strengthening Behavior of Magnesium Alloy Utilizing Nanoindentation. *J. Chongqing Univ. Technol. (Nat. Sci.)* **2020**, *34*, 141–146.
35. Hernández, S.G.; García, V.C.; Luna, E.L.; Vidal, M.A. Elastic modulus and hardness of cubic GaN grown by molecular beam epitaxy obtained by nanoindentation. *Thin Solid Films* **2020**, *699*, 137915. [[CrossRef](#)]
36. Hua, W.; Wu, X.; Shen, D.; Lu, H.; Polak, M. Nanohardness and elastic modulus at the interface of TiC_x/Ni₃Al composites determined by the nanoindentation technique. *Appl. Surf. Sci.* **2022**, *189*, 72–77. [[CrossRef](#)]
37. Cannon, W.R.; Sherby, O.D. High temperature creep behavior of class I and class II solid solution alloys. *Metall. Trans.* **1970**, *1*, 1030–1032. [[CrossRef](#)]
38. Günen, A.; Döleker, K.M.; Korkmaz, M.E.; Gök, M.S.; Erdogan, A. Characteristics, high temperature wear and oxidation behavior of boride layer grown on nimonic 80A Ni-based superalloy. *Surf. Coat. Technol.* **2021**, *409*, 126906. [[CrossRef](#)]
39. Zhou, L.; Mehta, A.; Cho, K.; Sohn, Y. Composition-dependent interdiffusion coefficient, reduced elastic modulus and hardness in γ , γ' and β -phases in the Ni-Al system. *J. Alloys Compd* **2017**, *727*, 153–162. [[CrossRef](#)]
40. Zhu, W.; Wu, Q.; Yang, L.; Zhou, Y.C. In situ characterization of high temperature elastic modulus and fracture toughness in air plasma sprayed thermal barrier coatings under bending by using digital image correlation. *Ceram. Int.* **2020**, *46*, 18526–18533. [[CrossRef](#)]
41. Hu, C.; Zhang, Z.; Chen, H.; He, J.; Guo, H. Reactive elements dependence of elastic properties and stacking fault energies of γ -Ni, γ' -Ni₃Al and β -NiAl. *J. Alloys Compd* **2020**, *843*, 155799. [[CrossRef](#)]